We are IntechOpen,
the world's leading publisher of
Open Access books
Built by scientists, for scientists

6,900
Open access books available

186,000
International authors and editors

200M
Downloads

Our authors are among the

154
Countries delivered to

TOP 1%
most cited scientists

12.2%
Contributors from top 500 universities

BOOK CITATION INDEX
CLARIVATE ANALYTICS
INDEXED

WEB OF SCIENCE™

Selection of our books indexed in the Book Citation Index
in Web of Science™ Core Collection (BKCI)

Interested in publishing with us?
Contact book.department@intechopen.com

Numbers displayed above are based on latest data collected.
For more information visit www.intechopen.com

Synthesis of High-Purity Ceramic Nano-Powders Using Dissolution Method

Suminar Pratapa, Ella A.D. Kiswanti, Dien R. Diana,

Yufi Hariyani, Lisma D.K. Sari, Musyarofah Musyarofah,

Triwikantoro Triwikantoro and Malik A. Baqiya

Abstract

A set of ceramic powders has been synthesized using a "bottom-up" approach which is denoted here as the dissolution method. The raw materials were metal powders or minerals. The dissolution media were strong acid or base solutions. In the case of metallic raw materials, magnesium and titanium powders were separately dissolved in hydrochloric acid to obtain their precursors. They were then dried, washed, and calcined in air at various temperatures to produce pure MgO and TiO_2 nano-powders. Pure $MgTiO_3$ nano-powders by mixing the precursors at the stoichiometric ratio and calcining the dried mixture at a temperature as low as 700°C have also been successfully synthesized. In the mineral case, local zircon sand was used as the raw material. A standard procedure to extract the "clean" and pure zircon powder was applied which included washing, magnetic separation, and reactions using hydrochloric acid and sodium hydroxide. A pure zircon nano-powder was obtained by applying mechanical ball-milling to the zircon powder. The zircon powder was also chemically dissociated to give amorphous silica (SiO_2), cristobalite, amorphous zirconia (ZrO_2), and nanometric tetragonal zirconia powders.

Keywords: dissolution method, strong acid and base, metal and mineral, ceramic nano-powders

1. Introduction

Many efforts have been paid to produce nano-powders since they exhibit different and usually outstanding physical and chemical properties as compared to their larger counterparts. Ceramic nano-powders are even more attractive since they are thermally and chemically more stable than non-ceramic ones. Several applications of such nano-powders are in drug delivery, corrosion inhibitor, catalyst, and microwave communication. Oxide ceramics such as MgO, TiO_2, $MgTiO_3$, ZrO_2, and SiO_2 are more abundant than non-oxide ceramics. Their use in technological and industrial applications is hence more substantial.

Oxide ceramic powders are not easily found in nature in their simple mono- and bi-cationic forms. Yet, their technological benefits are very valuable. Their existence in nature is usually in the form of complex compounds and needs further

processing to achieve high-purity substances. Furthermore, natural nano-ceramic powders are hardly found. As a result, various approaches have been proposed to synthesize such materials. Two general ways were usually used, that is, bottom-up and top-down methods. The former requires precursors of the desired cation(s) and usually uses heating in air or oxygen-controlled environment to develop the ceramics. The latter is basically a "breakdown" approach of a larger ceramic grains or particles by milling.

By definition, a nanometric powder means it has crystallite or grain or particle size less than 100 nm, although some researchers claimed that sub-nanometric size of <200 nm was still acceptable.

Several examples of synthesis of oxide nano-ceramic powders are solvothermal, sol-gel, and (co-)precipitation methods. The solvothermal involves the use of (usually) nonaqueous precursors and an autoclave to produce nanoparticles with unique microstructures. This method, for example, has been used to produce nanorods [1, 2], nanoclusters [3], and hollow spheres [4]. It is, however, a complex procedure. Meanwhile, the sol-gel method includes the use of complex precursors as the raw materials. For instance, synthesis of nanoparticles of magnesium and titanium oxides [5–8] has been reported recently. Despite its potential in controlling the size and shape of the products, the sol-gel process usually is time-consuming and costly. Finally, the precipitation or coprecipitation method has been reported by several researchers as an effective method to produce magnesia, titania (anatase), and zircon nano-powders [9–11]. The use of a precursor, washing with a certain liquid (usually distilled water), drying in air, and calcination are basic attributes in coprecipitation synthesis. The crystallite size of the synthesized powders for each method depends on many factors, particularly the type of precursors, as well as media, time, and temperature for processing. Some examples of nano-ceramics synthesized by these methods are presented in **Table 1**. Examples of bi-cationic ceramic nano-powders are also given.

Recently, an approach to processing oxide nano-ceramic powders has been developed. The approach, here designated as the dissolution method, comprises dissolution of a raw powder into a strong acid, followed by drying and washing, and finally calcination in air. There were several pure metals and minerals under our

Nano-material	Precursor	Method	Calcination temperature (°C)	Crystallite size (nm)	Refs.
MgO	$Mg(NO_3)_2.6H_2O$	Sol-gel	500	30	[5]
	$MgCl_2$	Sol-gel	800	100	[12]
	$Mg(CH_3COO)_2.4H_2O$	Solid	800	53	[13]
TiO_2	Tetrabutyl titanate	Sol-gel	160	6	[14]
	Titanium tetraisopropoxide	Sol-gel	500	30	[15]
	$TiOSO_4/CO(NH_2)_2$	Hydrothermal	1000	9	[10]
$MgTiO_3$	$Ti(OH)_4$ + Mg $(NO_3)_2.6H_2O$	Coprecipitation	700	30–40	[16]
	Mg $(NO_3)_2·6H_2O$ + Ti $[OCH(CH_3)_2]_4$	Sol-gel	400	12	[17]
Mg_2SiO_4	$(CH_3COO)_2Mg.4H_2O$ and $C_8H_{20}O_4Si$	Sol-gel	900	33	[18]

Table 1.
Methods to produce mono- and bi-cationic oxide nano-ceramics from references.

study. In terms of synthesis of nano-materials, it is also classified as a "bottom-up" approach and a wet method.

The report of the synthesis is arranged by the type of the raw materials, that is, metal and mineral. The metal powders were magnesium and titanium, which produced magnesia, titania, and magnesium titanate nano-powders. The second group materials were synthesized with a slightly different way, that is, there were cleaning and demagnetization to improve the "purity" of the raw material. Further approaches were used to obtain nanometric zircon, silica, and zirconia powders. The success of the syntheses was affirmed by analytical methods like thermogravimetric and differential thermal analyses, X-ray fluorescence spectroscopy, X-ray diffractometry, and high-resolution transmission electron microscopy.

2. Dissolution method

In principle, dissolution of solids into a liquid or other solvents is a process by which the original states become dissolved components (solutes), hence forming a solution of the solid in the original solvent (see the schematic diagram in **Figure 1**). When a dissolution occurs, the dissolved component separates into ions or molecules, and each of them is surrounded by the molecules of the solvent. Using the dissolution process, one can generate a precursor of a cation from a metal or a mineral if it is soluble in a selected (strong) acid. For example, magnesium reacts with hydrochloric acid according to $Mg(s) + 2HCl(aq) \rightarrow MgCl_2 (aq) + H_2(g)$ where the hydrogen gas is released [19]. On the other hand, titanium is a rather unreactive metal, making it difficult to dissolve unless more external energy such as heat is provided. Dissolving titanium powder in hydrochloric acid is possible as long as the process is run at approximately 60–70°C where the product is a purple solution of titanium trichloride.
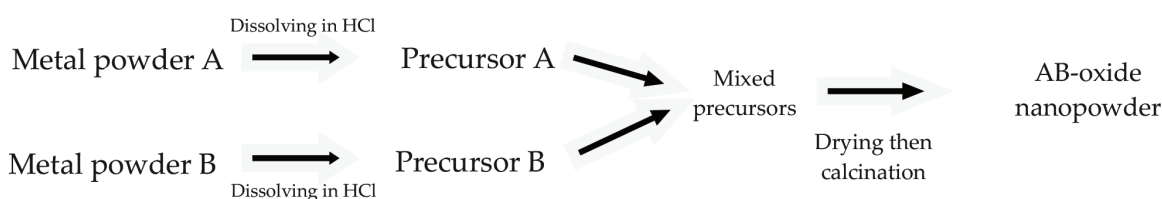

Figure 1.
Schematic diagram for dissolution process, an example for separate dissolution of A and B powders in HCl to synthesize AB oxide nano-powder.

Dissolution of metal oxide MO is also possible [20, 21], where M denotes a metal. Several factors may affect the dissolution kinetics including physical form and constitution of the oxides, as well as pH (acid or base), redox potential, chelating strength, concentration, and temperature of the solution. Examples of metal oxide dissolution in strong acids are for lanthanum oxide [22], iron oxides [23], and zinc ferrite [24]. In this work, the dissolution method was further used for selectively extracting the cations from natural mineral to produce high-purity ceramic nano-powders.

3. Synthesis and phase analyses of the powders

Tables 2 and **3** present a series of metal oxide powders which were produced by metal and mineral dissolutions, respectively. For the metal-dissolved powders, hydrochloric acid was used as the solvent. The oxide precursors were obtained by

Metal powder	Acid/ base	Precursor	Calcination temperature (°C)	Product	Crystallite size (nm)
Mg	HCl	$MgCl_2$	700	Pure MgO	98
Ti	HCl	$TiCl_4$	200 < T < 700	TiO_2 anatase	96–114
				TiO_2 rutile	6–96
			>800	TiO_2 rutile	>200
Ti Mg	HCl	Mixture of $TiCl_4$ and $MgCl_2$	700	Pure $MgTiO_3$	65

Table 2.
Dissolution of metal powders in acid to produce nanocrystalline oxide powders.

drying the precipitates after subsequent washing with water. The solvent for processing zircon sand, as shown in **Table 3**, depends on the purposed powder. Zircon sand can be processed to obtain nano-zircon, silica, or nano-zirconia powders. The calcination temperatures were selected after inspecting the thermal data from the precursors.

The structure, composition, and nanocrystallinity of the powders were examined using CuKα X-ray diffraction (XRD) data to which the Rietveld-based *Rietica* [25] and Material Analysis Using Diffraction (*MAUD*) [26] softwares were employed. The former was applied for phase composition calculation according to the "ZMV" method, while the latter for average crystallite size estimation by implementing the Thomson-Cox-Hastings [14] model in a pseudo-Voigt peak-shape function after instrumental correction using an annealed Y_2O_3 as suggested previously.

The relative weight fraction of phase *i* at each depth was determined by:

$$W_i = \frac{s_i(ZMV)_i}{\sum_{j=1}^{n} s_j(ZMV)_j} \quad (1)$$

where s_i denotes the Rietveld scale factors of sample *i* and *n* is the number of the phases. Z_i is the number of formula unit of phase *i* (calculated from the refined lattice parameters) with mass M_i in the unit cell volume V_i.

Mineral	Acid/base	Precursor/ precipitate	Calcination temperature (°C)	Product	Crystallite size (nm)
$ZrSiO_4$ (zircon sand)	NaOH	Na_2SiO_3	100 (drying)	Am. SiO_2	—
	HCl	Na_2SiO_3	900	Cristobalite	>500
	Milling in ethanol	—	100 (drying)	$ZrSiO_4$	160[a] 40[b]
	NaOH + HCl	$ZrOCl_2$	700	ZrO_2	20

[a]*Unmilled powder.*
[b]*Milled powder for 10 h at 150 rpm.*

Table 3.
Dissolution of natural zircon mineral to produce high-purity oxide powders.

High-resolution transmission electron microscope (TEM) was used to investigate the crystallite and particle sizes as well as the morphology of the synthesized powders.

3.1 Magnesium oxide (MgO)

The dried powder of Mg-dissolved solution was run for DTA/TG characterization where the associated plot is given in **Figure 2**. A significant drop of the mass of the powdered sample between RT and approximately 600°C is related to some thermodynamic phenomena recorded as endothermic peaks. The peaks between RT and 300°C are attributed to release water molecules with a mass loss of approximately 50%, while the peak at ∼500°C is due to the liberation of chloride ions and molecules. The last release is also indicated by some mass drop up to 600°C. The DTA/TG observations led the synthesis of MgO. A calcination temperature range of 400–800°C was then selected. The success of the syntheses was examined mainly using XRD measurements (**Figure 3**).

The XRD patterns of the calcined Mg-dissolved powders clearly show the phase evolution with calcination temperature. At 400°C, only bischofite ($MgCl_2 \cdot 6H_2O$) was detected. Increasing the temperature to 500°C resulted in the formation of MgO, and further calcination at 700°C gave pure MgO. This result indicates that between 400 and 700°C, there was a reaction of $MgCl_2 \cdot 6H_2O$ (s) → MgO (s) + H_2O (g) + Cl_2 (g). As implied by the DTA/TG data, there is a drop of mass and exothermic phenomena which can be ascribed to this reaction. Further analysis shows that the composition and crystallite size of the products change subsequently (**Table 4**). Therefore, the Mg metal-dissolved method can produce nanocrystalline, pure MgO powder after calcination at 700°C. Calcination at 800°C does not significantly alter the phase characteristics of the powder.

3.2 Titanium dioxide (TiO_2)

DTA/TG plot of the dried Ti-dissolved solution is given in **Figure 4**. The XRD patterns of the calcined powders are presented in **Figure 5**. Similar behavior in the phase formation of MgO was found here for the Ti-dissolved powders. Significant mass release occurs and followed by crystallite formation. Interestingly, the dried Ti-dissolved powder has already exhibited rutile with a relatively low degree of crystallinity as indicated by low diffraction intensities. The crystallinity becomes clearer at higher calcination temperatures. Pure rutile is achieved at 400°C, but anatase forms above 600°C. In most cases, the formation of anatase occurs at a
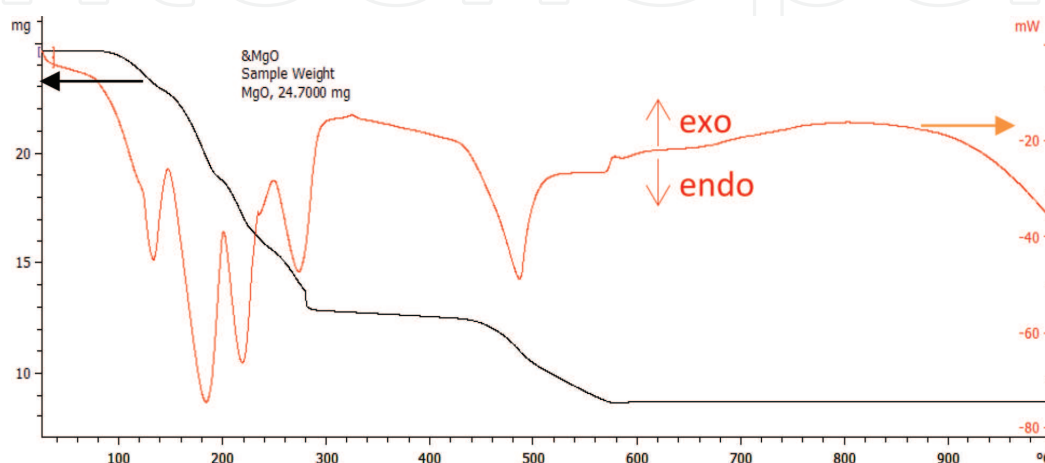

Figure 2.
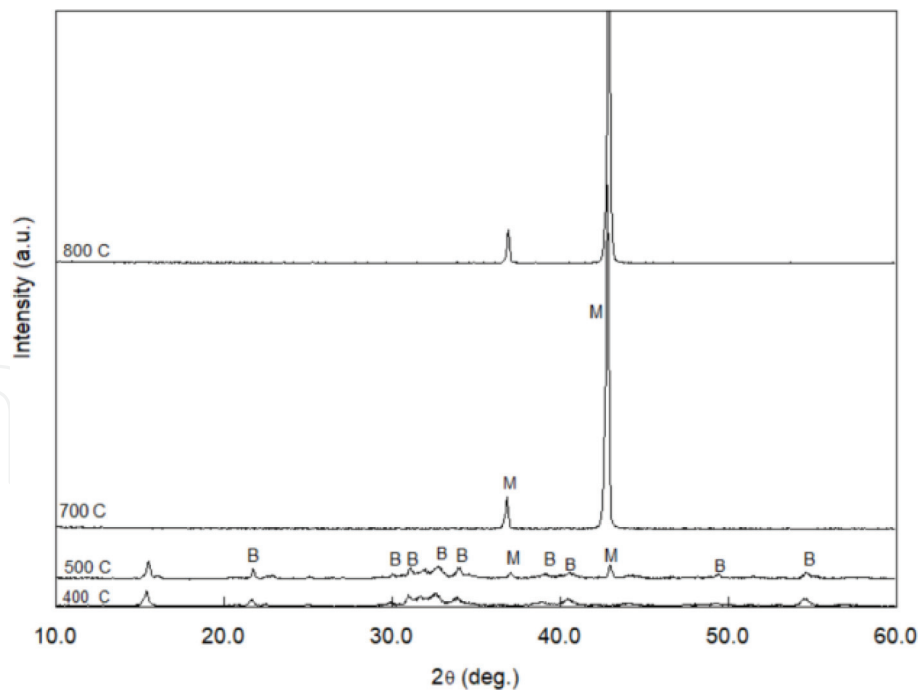*DTA/TG plot of the Mg-dissolved dried powder.*

Figure 3.
X-ray diffraction patterns (CuKα radiation) of the calcined Mg-dissolved powders. Symbols: B = bischofite ($MgCl_2 \cdot 6H_2O$), M = magnesia (MgO, also known as periclase).

Temperature	Weight fraction (%)		Crystallite size (nm)	
	MgO (periclase)	$MgCl_2.6H_2O$ (bischofite)	MgO (periclase)	$MgCl_2.6H_2O$ (bischofite)
400°C	—	100	—	90(12)
500°C	18.5	81.5	99(5)	97(5)
700°C	100	—	98(5)	—
800°C	100	—	98(3)	—

Table 4.
Phase weight fraction and MgO crystallite size of the calcined Mg-dissolved powders extracted from XRD data.
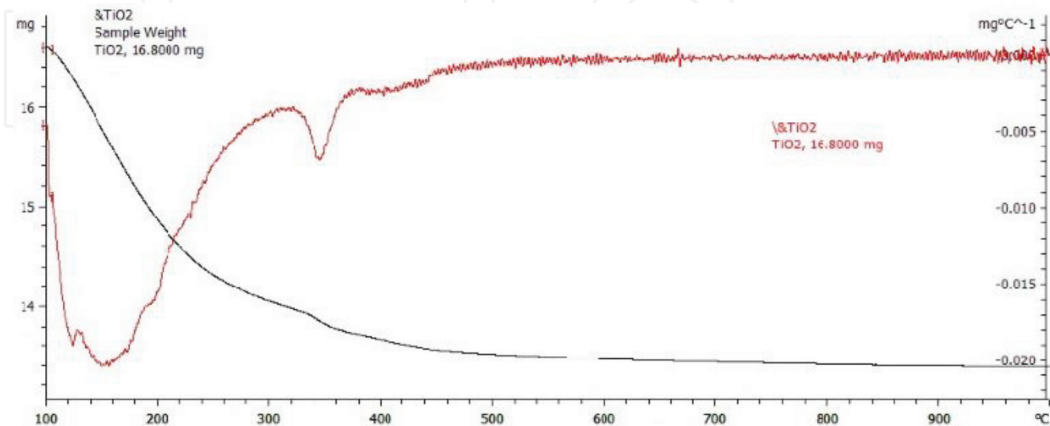
Figure 4.
DTA/TG plot of the Ti-dissolved dried powder.

lower temperature than rutile [8, 10]. In our study, the formation of rutile is more spontaneous than anatase possibly due to the type of precursor and its environment. A similar result was observed by others [27]. It is also worth noting that the broad
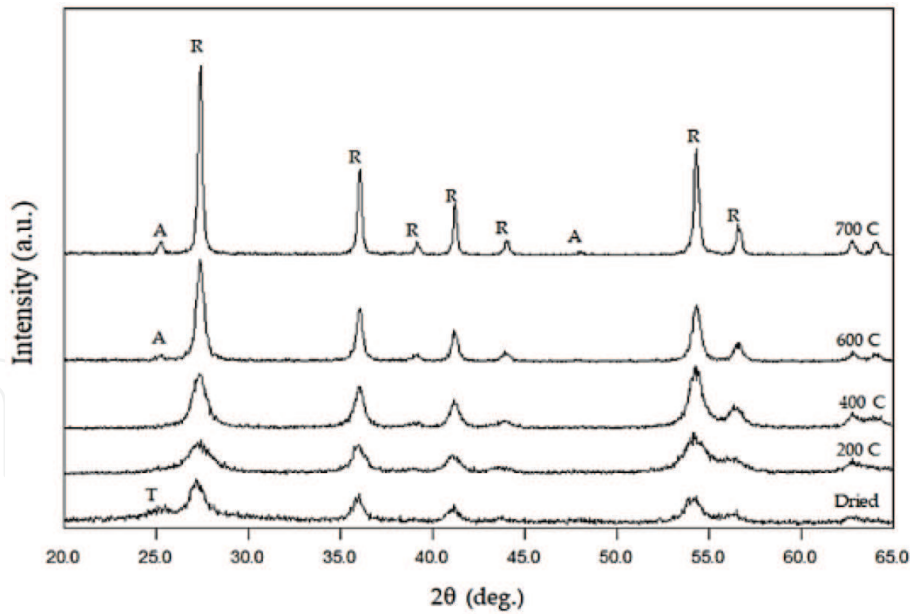
Figure 5.
X-ray diffraction patterns (CuKα radiation) of the calcined Ti-dissolved powders. Symbols: A = TiO$_2$ anatase, R = TiO$_2$ rutile, T = undetected phase.

Temperature (°C)	Relative weight fraction (%)		Crystallite size (nm)	
	Rutile	**Anatase**	**Rutile**	**Anatase**
200°C	100	—	6 (1)	—
400°C	100	—	11(1)	—
600°C	97.96(5)	2.04(1)	22(1)	98(2)
700°C	99.08(5)	0.92(1)	96(3)	114(6)

Table 5.
Phase weight fraction and TiO$_2$ crystallite size of the calcined Ti-dissolved powders extracted from XRD data.

XRD peaks imply the nanometric crystal size of the products [28]. MAUD software [26] estimated crystallite size of rutile and anatase in the samples which are presented in **Table 5**.

3.3 Magnesium titanium oxide or magnesium titanate (MgTiO$_3$)

Synthesis of MgTiO$_3$ powder can be performed following the schematic diagram given in **Figure 2**. The detailed explanation of the synthesis has been reported elsewhere [29]. In principle, the magnesium powder was dissolved in hydrochloric acid at room temperature stirring to obtain a light yellow solution, while the titanium powder was prepared similarly but at around 60°C to give a purple solution. Both solutions were then stirred at around 75°C for 4 h to ensure homogenous mixing prior to drying at 105°C to produce granular agglomerates. Phase and microstructure analyses were performed on the manually ground agglomerates after calcination at various temperatures. **Figure 6** shows the XRD patterns of calcined powders for 1:1 Mg:Ti ratio at different temperatures. As can be seen from the figure, only MT (COD ID 01-079-0831, hexagonal), MgO (periclase, 00-045-0946, cubic), and rutile (01-078-2485, tetragonal) were present in all samples. This result shows that our dissolution method can hinder the formation of other magnesium titanate phases such as MgTi$_2$O$_5$ [30, 31] or Mg$_2$TiO$_4$ [32]. However, the
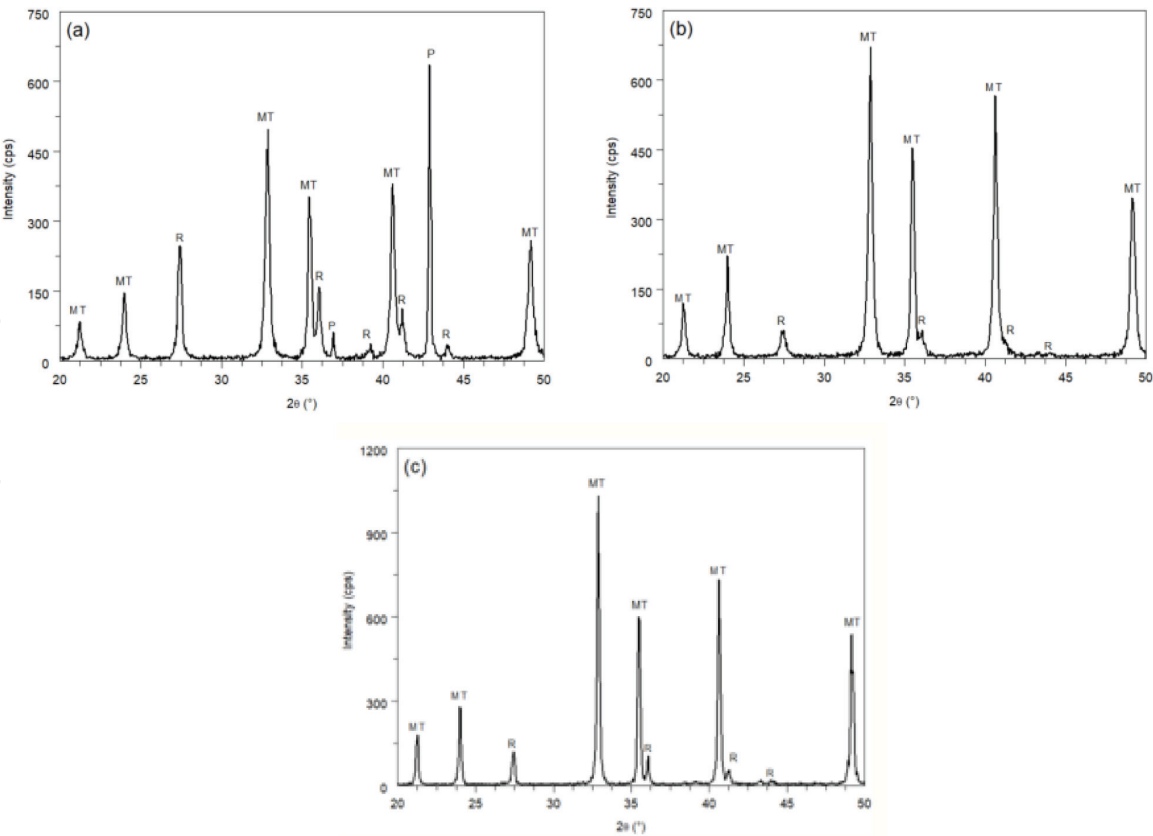
Figure 6.
X-ray diffraction patterns (CuKα radiation) of the calcined (Mg, Ti)-dissolved powders at various calcination temperatures: (a) 600, (b) 700, and (c) 800°C. symbols: MT = MgTiO₃, R = rutile, P = periclase (MgO).

presence of periclase and rutile shows that the product is not pure MT. In terms of XRD line peaks, the MT patterns exhibit broadened peaks, particularly at lower temperatures indicating that it is in nanometric crystallite size [17]. The average XRD crystallite size of the MT nanocrystals is between 76 ± 2 nm (600°C) and 150 ± 4 nm (800°C). **Figure 7** shows a typical TEM micrograph of the MT crystallites. The micrograph shows inhomogeneous crystallite size ranging between 50 and 120 nm—being the dominating size is around 80 nm. Therefore, the TEM result supports that of XRD, where the hexagonal morphology of the crystallites confirms
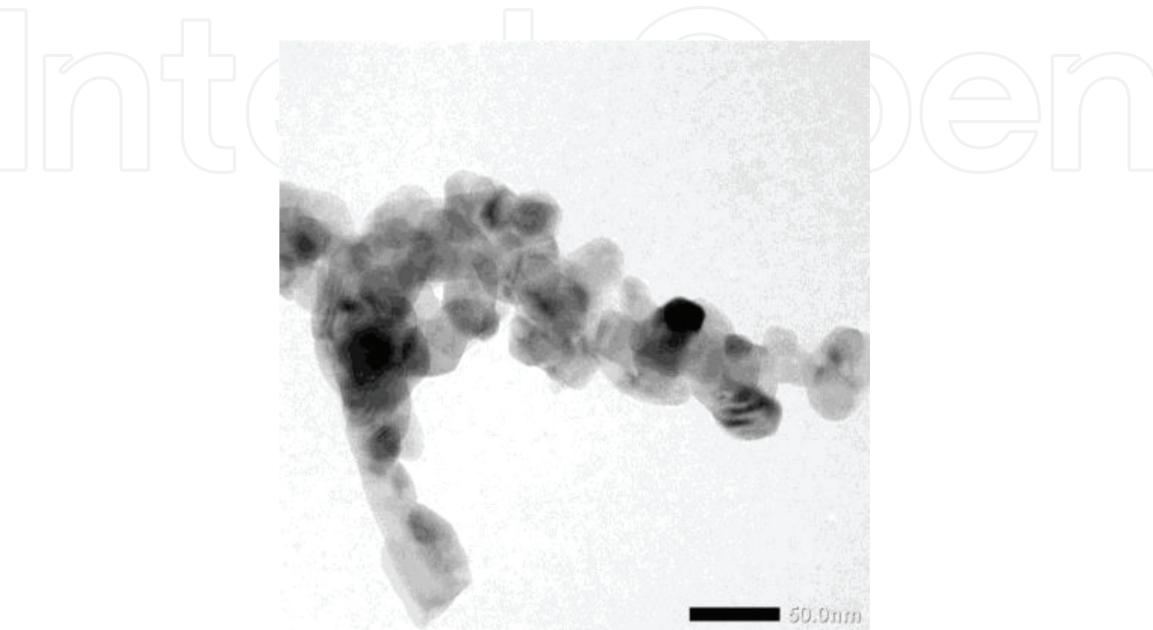

Figure 7.
TEM micrograph of MT powder after calcination at 600°C.

the structure of the phase. In conclusion, the simple dissolution method is very potential to produce bi-cationic nanocrystals.

3.3.1 Effect of excessive Mg

The influence of excessive Mg [33] to produce higher-purity MT was investigated further by XRD for samples which were calcined at 800°C [29]. It has been shown that excessive addition of Mg up to 3% reduces the amount of rutile (R), while above 6% addition causes vanishing rutile but the appearance of periclase (*M*). This result implies that the method can be easily used to control the amount of MT by varying Mg:Ti ratio without the introduction of $MgTi_2O_5$ or Mg_2TiO_4 which was found when other methods were used [30, 32]. The results explained the role of excessive Mg in the formation of high-purity MT. The amount of MT can achieve as high as $99.4 \pm 3.6\%$ in the 6% excessive Mg sample with rutile as the sole residual or $97.5 \pm 3.5\%$ in the 3% excessive Mg sample with periclase as also the only residual. An excessive Mg around 5–6% is therefore envisaged to give MT with the highest purity [29].

3.3.2 Effect of calcination dwelling time

The formation of MT at 600°C with 1 h dwelling time was incomplete, with the weight fraction of rutile and periclase that was about 17.2 and 17.4%, respectively, while increasing calcination temperature improves such formation. The effect of calcination dwelling time on the completeness of the MT formation was then examined [29]. It was reported that the formation of MT is significantly improved by prolonged calcination as proven by the MT molar fraction around 65% (equivalent with around 82% by weight) for 1 h to 82% (90% by weight) for 4 h. It was also found that the crystallite size of MT was invariant to dwelling time at values around 76 nm as indicated by insignificant changes on the XRD line.

Therefore, the dissolution method has been successfully implemented to produce high-purity MT nanocrystals. Sub-nanometric MT crystals were achieved from Mg-Ti hydrochloric acid solutions mixing with 6% excessive Mg followed by calcination at 800°C for 1 h. Meanwhile, prolonged calcination at 600°C significantly improved the MT formation up to 82% (molar) and retained its nanometric crystallite size at around 76 nm.

3.4 Zircon ($ZrSiO_4$)

Synthesis of $ZrSiO_4$ powder was performed by making use of natural zircon sand which was collected from District of Kereng Pangi in Central Kalimantan. To obtain a pure zircon powder, the sand was subject to several processing steps including magnetic separation, reaction with HCl followed with NaOH, and finally washing and drying. The XRD patterns of the samples after each processing are presented in **Figure 8**. Several inferences can be drawn from the figure, for example, the dominating phase in the sand and powder is zircon ($ZrSiO_4$, COD ID 900-2554). Furthermore, the highest intensity increases with the processing step, indicating that the crystallinity improves subsequently. Moreover, the undetected peaks disappear after reacting the sand with HCl. Investigation using XRF showed that the disappearance of the undetected XRD peaks in Sample (B) could be associated with the removal of unwanted substances such as Ti and Fe in the sand (**Figure 9**). However, Sample (B) contains silica quartz (COD ID 500-0035). The XRF data showed Zr:Si weight fraction ratio of approximately 3:2 which indicates that pure zircon powder has not been achieved since the ratio should be at approximately 3:1. Reaction with
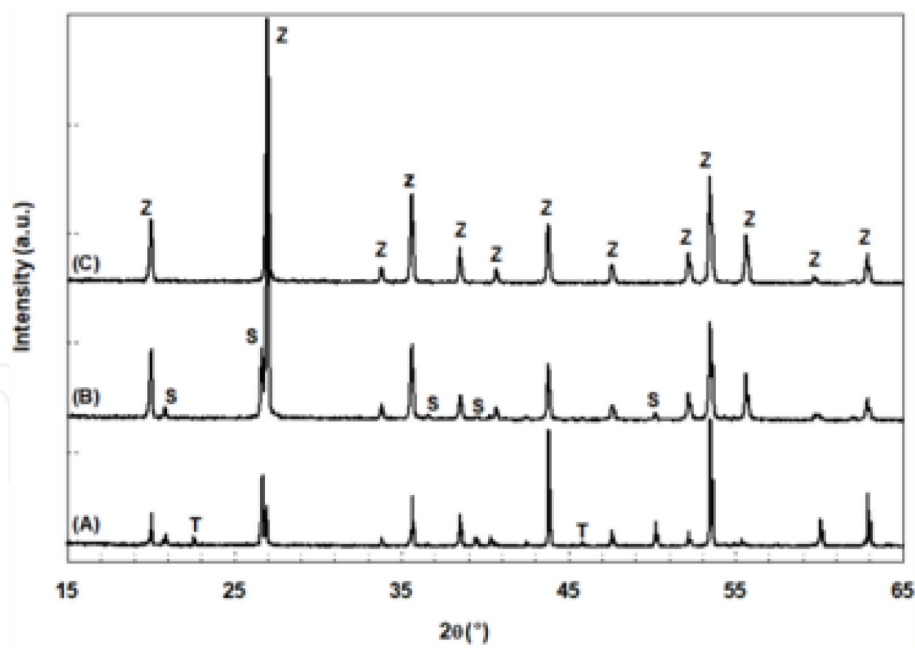
Figure 8.
X-ray diffraction patterns (CuKα radiation) of (A) zircon sand, (B) zircon powder after magnetic separation and reaction with HCl, and (C) powder B after reaction with NaOH and washing. Symbols: Z = zircon, ZrSiO₄; S = silica (SiO₂), quartz; T = undetected.
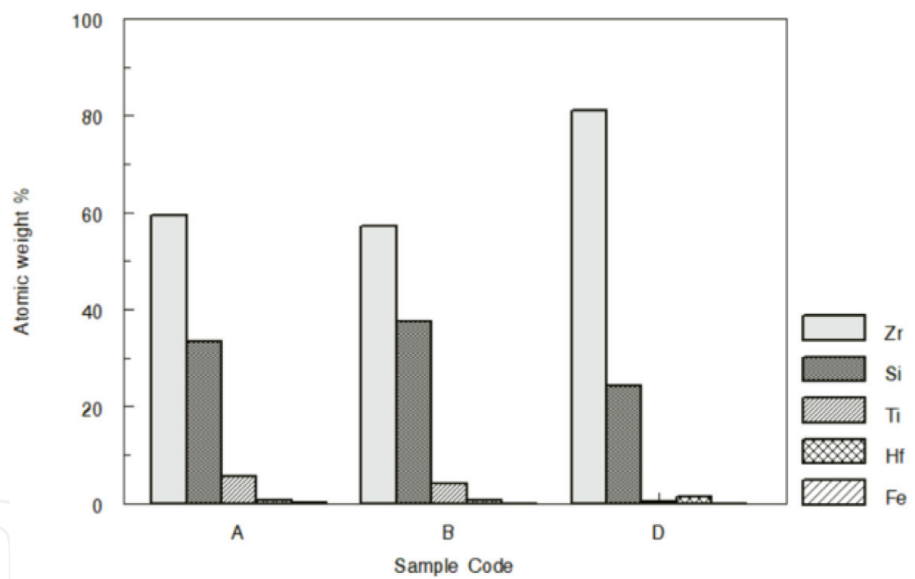

Figure 9.
X-ray fluorescence atomic weight fractions of (a) zircon sand, (B) zircon powder after magnetic separation and reaction with HCl, and (C) powder B after reaction with NaOH and washing.

NaOH was subsequently done to form liquid Na_2SiO_3 precursor which can be easily removed by sieving. The sieved slurry was then washed and dried to obtain pure zircon powder (Sample (C)). The SEM image and its energy-dispersive elemental mapping of Sample C are shown in **Figure 10**. The figures indicate the high crystallinity and high purity of the powder. These facts show that the dissolve method which comprises magnetic separation, HCl reaction, washing-filtering, NaOH reaction, another washing-filtering, and drying of natural zircon sand may produce high-purity, single-phase zircon powder.

An effort to process the zircon powder to achieve zircon nano-powder has been accomplished. The mechanical zirconia ball-milling was chosen. Well-sintered partially stabilized zirconia ceramics exhibit much higher Vickers' hardness than zircon
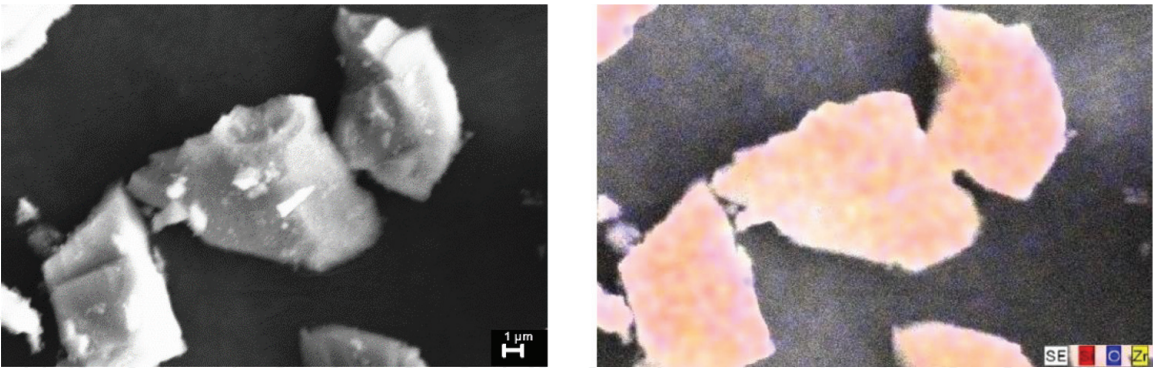
Figure 10.
SEM image (SEI mode, left) and its energy-dispersive elemental mapping (right) of the purified zircon powder (sample C).

ceramics, that is, 15 GPa [34] versus 3 GPa [35]. Therefore, zirconia balls would presumably be able to mill zircon powder. The XRD patterns of the milled zircon powders at various milling time are presented in **Figure 11**. Milling has no effect on the detected phase, that is, it remains zircon, and resulted in lower but broader peak intensity. The XRD peak broadening was caused by crystallite size and nonuniform effects after milling. These XRD characters were investigated using MAUD software [26] and came across at a conclusion that the synthesized zircon powder exhibited smaller crystallite size after milling, that is, from 173 nm before milling to 162 and finally to 45 nm after milling for 5 and 10 h, respectively. TEM images of the unmilled and 10 h milled zircon powders are shown in **Figure 12**. These images confirm the success of the synthesis of the nano-sized zircon powder.

The software also allowed the extraction of a nonuniform strain of the milled powder, and the results showed that longer milling induced more strains as also observed by others [36, 37] for different metal oxides. The strain values for the zircon powders are 2, 3, and 6×10^{-4} for the unmilled and 5 and 10 h for milled samples, respectively. These values dropped significantly to as low as 2×10^{-4} after annealing at 200°C for 2 h.
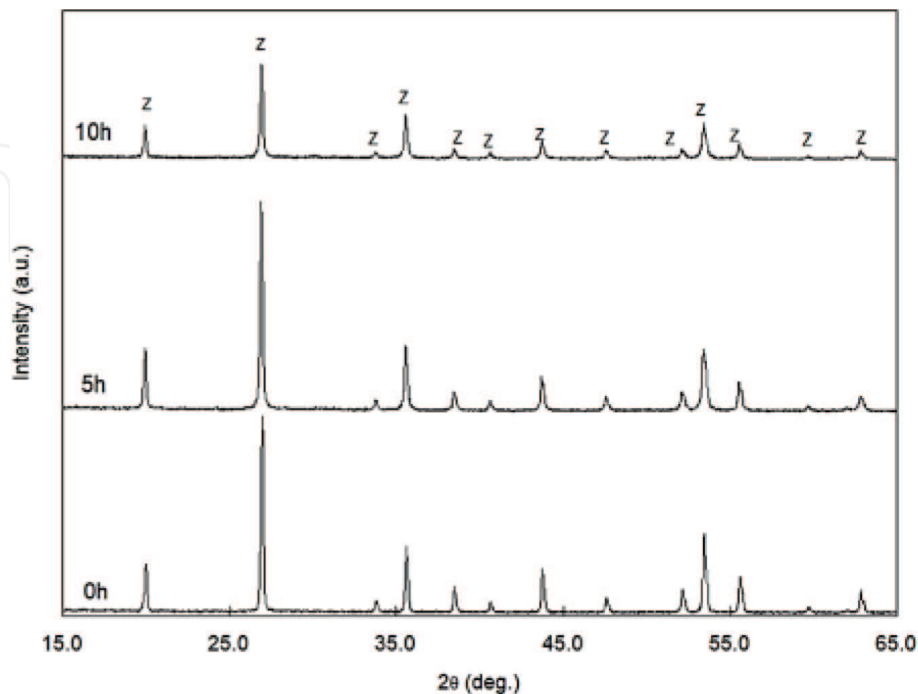

Figure 11.
X-ray diffraction patterns (CuKα radiation) of milled zircon powder at various milling times. Symbol: Z = zircon, $ZrSiO_4$.
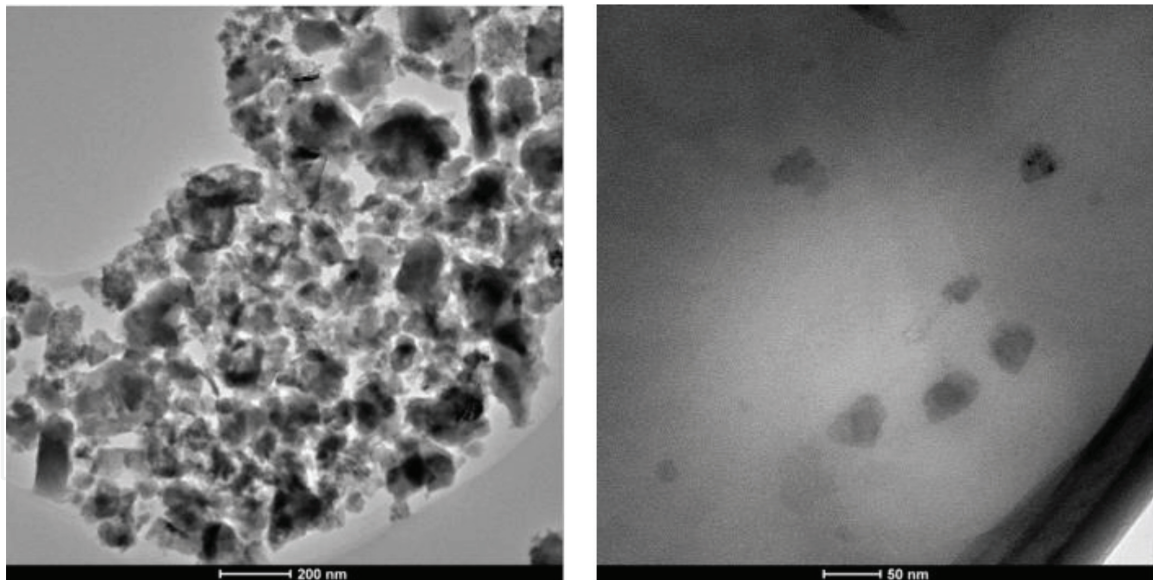
Figure 12.
TEM micrographs of unmilled (left) and 10 h milled zircon (right) powders.

4. Conclusion

It has been demonstrated that a simple dissolve method using HCl or NaOH which was reacted with a mono- or bi-cationic metals or with a natural mineral can be accomplished to produce high-purity, nanocrystalline metal oxide ceramics. Pure MgO, TiO_2, $MgTiO_3$, and $ZrSiO_4$ nano-powders were produced by the method. The main step for the metal case was on the formation of the precursor and appropriate calcination temperature. For the mineral case, purification of the phase under consideration by reacting the contaminating phase with acid or base, followed by filtering, washing, and calcination, was the key of the process.

Acknowledgements

Author details

Suminar Pratapa[1]*, Ella A.D. Kiswanti[1], Dien R. Diana[1], Yufi Hariyani[1], Lisma D.K. Sari[2], Musyarofah Musyarofah[1], Triwikantoro Triwikantoro[1] and Malik A. Baqiya[1]

1 Department of Physics, Faculty of Science, Institute of Technology Sepuluh Nopember (ITS), Surabaya, Indonesia

2 Study Program of Mathematics, STKIP PGRI, Situbondo, Indonesia

*Address all correspondence to: suminar_pratapa@physics.its.ac.id

IntechOpen

References

[1] Li T, Liao JP, Wang YF. Solvothermal synthesis and magnetic properties of β-Co_2P nanorods. Materials Science-Poland. 2015;**33**:312-316. DOI: 10.1515/msp-2015-0049

[2] Sin J-C, Lam S-M, Lee K-T, Mohamed AR. Surfactant-free solvothermal synthesis of ZnO nanorods for effective sunlight degradation of 2,4-dichlorophenol. Materials Letters. 2015;**140**:51-54. DOI: 10.1016/j.matlet.2014.10.067

[3] Chun J, Jo C, Lim E, Roh KC, Lee J. Solvothermal synthesis of sodium cobalt fluoride ($NaCoF_3$) nanoparticle clusters. Materials Letters. 2017;**207**:89-92. DOI: 10.1016/j.matlet.2017. 07.059

[4] Kurajica S, Minga I, Grčić I, Mandić V, Plodinec M. The utilization of modified alkoxide as a precursor for solvothermal synthesis of nanocrystalline titania. Materials Chemistry and Physics. 2017;**196**: 194-204. DOI: 10.1016/j.matchemphys.2017.04.064

[5] Tamilselvi P, Yelilarasi A, Hema M, Anbarasan R. Synthesis of hierarchical structured MgO by sol-gel method. Nano Bulletin. 2013;**2**:130106

[6] Soleimanian V, Aghdaee SR. X-ray diffraction analysis of the effect of annealing temperature on the microstructure of magnesium oxide nanopowder. Journal of Physics and Chemistry of Solids. 2015;**81**:1-9. DOI: 10.1016/j.jpcs.2014.12.020

[7] Jeevanandam J, Chan YS, Danquah MK. Calcination-dependent morphology transformation of sol-gel-synthesized MgO nanoparticles. ChemistrySelect. 2017;**2**:10393-10404. DOI: 10.1002/slct.201701911

[8] Dubey RS. Temperature-dependent phase transformation of TiO_2 nanoparticles synthesized by sol-gel method. Materials Letters. 2018;**215**: 312-317. DOI: 10.1016/j.matlet.2017. 12.120

[9] Shi Y, Huang X, Yan D. Synthesis and characterization of ultrafine zircon powder. Ceramics International. 1998; **24**:393-400. DOI: 10.1016/S0272-8842 (97)00027-8

[10] Ran FY, Cao WB, Li YH, Zhang XN. Preparation of nanosize anatase TiO_2 powders by hydrothermal synthesis. Key Engineering Materials. 2007; **336–338**:2017-2020. DOI: 10.4028/www.scientific.net/KEM.336-338.2017

[11] Rajendran V, Deepa B, Mekala R. Studies on structural, morphological, optical and antibacterial activity of pure and Cu-doped MgO nanoparticles synthesized by co-precipitation method. Materials Today: Proceedings. 2018;**5**: 8796-8803. DOI: 10.1016/j.matpr.2017.12.308

[12] Pei L-Z, Yin W-Y, Wang J-F, Chen J, Fan C-G, Zhang Q-F. Low temperature synthesis of magnesium oxide and spinel powders by a sol-gel process. Materials Research. 2010;**13**: 339-343. DOI: 10.1590/S1516-14392010000300010

[13] Kamarulzaman N, Chayed NF, Badar N. MgO nanoparticles via a simple solid-state reaction. In: International Symposium on Frontier of Applied Physics (ISFAP) 2015; 5-7 October 2015; Bandung: AIP Publishing. 2016;**1711**: p. 040004. DOI: 10.1063/1.4941626

[14] Cai W, Yang H, Guo X. A facile synthesis of nanocrystalline spherical TiO_2 particles and its photoluminescent properties. Procedia Engineering. 2014; **94**:71-75. DOI: 10.1016/j.proeng.2013.11.042

[15] Nachit W, Touhtouh S, Ramzi Z, Zbair M, Eddiai A, Rguiti M, et al. Synthesis of nanosized TiO_2 powder by sol gel method at low temperature. Molecular Crystals and Liquid Crystals. 2016;**627**:170-175. DOI: 10.1080/ 15421406.2015.1137135

[16] Parthasarathy G, Manorama SV. A novel method for synthesizing nano-crystalline $MgTiO_3$ geikielite. Bulletin of Materials Science. 2007;**30**:19-21. DOI: 10.1007/s12034-007-0004-y

[17] Kanna RR, Dhineshbabu NR, Paramasivam P, Rajendran V, Yuvakkumar R. Synthesis of geikielite ($MgTiO_3$) nanoparticles via sol–gel method and studies on their structural and optical properties. Journal of Nanoscience and Nanotechnology. 2016;**16**:7635-7641. DOI: 10.1166/ jnn.2016. 11114

[18] Tamin SH, Adnan SBRS, Jaafar MH, Mohamed NS. Effects of sintering temperature on the structure and electrochemical performance of Mg_2SiO_4 cathode materials. Ionics. 2017; **24**:2665-2671. DOI: 10.1007/s11581-017-2391-4

[19] Roald B, Beck W. The dissolution of magnesium in hydrochloric acid. Journal of the Electrochemical Society. 1951;**98**: 277. DOI: 10.1149/1.2778207

[20] Wellens S, Vander Hoogerstraete T, Möller C, Thijs B, Luyten J, Binnemans K. Dissolution of metal oxides in an acid-saturated ionic liquid solution and investigation of the back-extraction behaviour to the aqueous phase. Hydrometallurgy. 2014;**144–145**:27-33. DOI: 10.1016/j.hydromet.2014.01.015

[21] Casey WH, Ludwig C. The mechanism of dissolution of oxide minerals. Nature. 1996;**381**:506-509. DOI: 10.1038/381506a0

[22] Pinto AH, Souza FL, Chiquito AJ, Longo E, Leite ER, Camargo ER. Characterization of dense lead lanthanum titanate ceramics prepared from powders synthesized by the oxidant peroxo method. Materials Chemistry and Physics. 2010;**124**: 1051-1056. DOI: 10.1016/j. matchemphys.2010.08.030

[23] Shabashov VA, Sagaradze VV, Litvinov AV, Mukoseev AG, Vildanova NF. Mechanical synthesis in the iron oxide—Metal system. Materials Science and Engineering A. 2005;**392**:62-72. DOI: 10.1016/j.msea.2004.11.006

[24] Reutov DS, Khalezov BD, Ovchinnikova LA, Gavrilov AS. Investigation of zinc ferrite dissolution kinetics by roll-disc method. Tsvetnye Metally. 2017;**11**:12-15. DOI: 10.17580/ tsm.2017.11.02

[25] Hunter BA. Rietica. International Union of Crystallography Commission on Powder Diffraction Newsletter. 1998; **20**:21

[26] Lutteroti L. MAUD: Material Analysis Using Diffraction. Availble from: http://maud.radiographema.eu/ [Accessed: Aug 25, 2018]

[27] Samuel V, Pasricha R, Ravi V. Synthesis of nanocrystalline rutile. Ceramics International. 2005;**31**:555-557. DOI: 10.1016/j.ceramint.2004.07.003

[28] Pratapa S, Susanti L, Insany YAS, Alfiati Z, Hartono B, Mashuri A, et al. XRD line-broadening characteristics of M-oxides (M = Mg, Mg-Al, Y, Fe) nanoparticles produced by coprecipitation method. In: Proceedings of the Third Nanoscience and Nanotechnology Symposium (NNSB2010); 16 June 2010; Bandung: AIP Publishing. 2010;**1284**:125-128

[29] Pratapa S, Baqiya MA, Istianah I, Lestari R, Angela R. A simple dissolved metals mixing method to produce high-purity $MgTiO_3$ nanocrystals. In: Proceedings of the Fifth Nanoscience

and Nanotechnology Symposium (NNS2013); 23-25 October 2013; Surabaya: AIP Publishing. 2014;**1586**: 39-42. DOI: 10.1063/1.4866726

[30] Bernard J, Belnou F, Houivet D, Haussonne J-M. Synthesis of pure $MgTiO_3$ by optimizing mixing/grinding condition of $MgO + TiO_2$ powders. Journal of Materials Processing Technology. 2008;**199**:150-155. DOI: 10.1016/j.jmatprotec.2007.07.044

[31] Tang B, Zhang S, Zhou X, Deng C, Yu S. Preparation of pure $MgTiO_3$ powders and the effect of the $ZnNb_2O_6$-dope onto the property of $MgTiO_3$-based ceramics. Journal of Alloys and Compounds. 2010;**492**:461-465. DOI: 10.1016/j.jallcom.2009.11.140

[32] Miao Y-M, Zhang Q-L, Yang H, Wang H-P. Low-temperature synthesis of nano-crystalline magnesium titanate materials by the sol-gel method. Materials Science and Engineering B. 2006;**128**:103-106. DOI: 10.1016/j. mseb.2005.11.019

[33] Sreedhar K, Pavaskar NR. Synthesis of $MgTiO_3$ and $Mg_4Nb_2O_9$ using stoichiometrically excess MgO. Materials Letters. 2002;**53**:452-455. DOI: 10.1016/S0167-577X(01)00525-0

[34] Hirano M, Inada H. Fracture toughness, strength and Vickers hardness of yttria-ceria-doped tetragonal zirconia/alumina composites fabricated by hot isostatic pressing. Journal of Materials Science. 1992;**27**: 3511-3518. DOI: 10.1007/BF01151827

[35] Rendtorff NM, Grasso S, Hu C, Suarez G, Aglietti EF, Sakka Y. Dense zircon ($ZrSiO_4$) ceramics by high energy ball milling and spark plasma sintering. Ceramics International. 2012; **38**:1793-1799. DOI: 10.1016/j. ceramint.2011.10.001

[36] Indris S, Bork D, Heitjans P. Nanocrystalline oxide ceramics

prepared by high-energy ball milling. Journal of Materials Synthesis and Processing. 2000;**8**:245-250. DOI: 10.1023/A:1011324429011

[37] Ekström T, Chatfield C, Wruss W, Maly-Schreiber M. The use of X-ray diffraction peak-broadening analysis to characterize ground Al_2O_3 powders. Journal of Materials Science. 1985;**20**: 1266-1274. DOI: 10.1007/BF01026322